Modulating Blue Phosphorene by Synergetic Codoping: Indirect to Direct Gap Transition and Strong Band Gap Bowing

Xiaoqing Tian, Jingyi Duan, Yadong Wei, Naixing Feng, Xiangrong Wang,* Zhirui Gong, Yu Du,* and Boris I. Yakobson*

Prof. Dr. X. Q. Tian, J. Y. Duan, Prof. Dr. Y. D. Wei, Prof. Dr. Z. R. Gong, Prof. Dr. Y. Du,

College of Physics and Energy

Shenzhen University

Shenzhen, Guangdong 518060, China

Email: duyu@szu.edu.cn

Prof. Dr. N. X. Feng,

College of Electronic Sciences and Technology

Shenzhen University

Shenzhen, Guangdong 518060, China

Prof. Dr. X. Q. Tian, Prof. Dr. X. R. Wang

Department of Physics

The Hong Kong University of Science and Technology,

Clear Water Bay, Kowloon, Hong Kong

Email: phxwan@ust.hk

Prof. Dr. B. I. Yakobson

Department of Materials Science and NanoEngineering

Rice University, Houston, TX 77005 (USA)

This is the author manuscript accepted for publication and has undergone full peer review but has not been through the copyediting, typesetting, pagination and proofreading process, which may lead to differences between this version and the Version of Record. Please cite this article as doi: 10.1002/adfm.201808721.

E-mail: biy@rice.edu

We investigate the structural and electronic properties of synergeticly modified blue phosphorene (BP). The inversion and three-fold rotational symmetries of BP are broken. The co-doping of group IV and VI impurities can turn monolayer BP into direct band gap semiconductors. The underlying physical mechanism is that group IV and VI impurities tailor the valence band maximum and conduction band minimum respectively and move them to Γ. All the band gaps of monolayer, nanoribbons and quantum dots of BP can be modulated in a wide range, and the strong band Gap bowing is found. In addition the Coulomb interactions between the screened impurities are revealed. Lower formation energies indicate the fabricating practicability of synergeticly modified BP. Spin-orbit coupling (SOC) can also be tuned by the introduction of impurities.

1. Introduction

Blue phosphorene (BP), which was theoretically predicted to be an indirect band gap semiconductor with the stability comparable to black phosphorene[1], has been recently synthesized in the experiments.[2] BP has the layered hexagonal honeycomb structure and each monolayer is composed of two atomic layers. It can be easily exfoliated from the bulk due to the weak interlayer van der Waals interactions. The structure of BP is mixed of sp^2 and sp^3 character similar to that of silicene.[3] Compared to black phosphorene, the BP has a smaller unit cell and intralayer buckling. The band gap of BP is around 0.9 eV larger than that of black phosphorene. The mono-elemental characteristic can guarantee the low defect concentration and simple device fabrication process. However, the indirect band gap characteristic will hinder the applications of BP in optoelectronic and electronic devices.

There is little report on experimentally modulating electronic structures of BP although several techniques have been used to modulate the electronic structures of the two-dimensional allotrope of BP, black phosphorene. Uniaxial and biaxial strain and vertical deformation are used to tune the electronic structures of black phosphorene, and the semiconductor to metal transition was observed.[4] Noble-metal elements and alkali-metal elements such as Cu, Au, Pt, K and Na were used to dope black phosphorene. The structure stacking transition from AB to AC transition, n-type doping on phosphorene, and anisotropic Dirac semimetal properties were realized by the metal surface doping or incorporation.[5] Doping and annoying are the generic method for the band gap

engineering of traditional and 2D semiconductors.[6,7] Group-IV direct band gap ternary alloy was realized.[7d] Through the heavy impurities doping, the spin-orbit-coupling (SOC) in semiconductors can be engineered and even the giant SOC bowing was realized.[7e] Here we use first-principles method to study the band structure engineering of BP by synergetic modification. The codoping of group IV and VI impurities can turn BP into direct band gap semiconductors. Recently, two-dimensional IV-VI binary semiconductors have also been synthesized in the experiments. [8]

2. Computational Methods

Theoretical calculations were performed within the Quantum Espresso package.[9] The Perdew-Burke-Ernzerh (PBE) type of generalized gradient approximation exchange correlation functional was used.[10] 500 eV was used as the plane-wave basis set cutoff. The energy convergence criterion for the electronic wave function was set to be 10^{-6} eV. The geometry optimization was considered to be converged when the residual force on each atom was smaller than 1×10^{-3} eV/Å. A 20 Å thick vacuum layer normal to the plane was used to eliminate longitudinal interactions between the super cells. The BP 8×8 supercell was used for the calculations. The 6×6×1 Monkhorst-Pack k-point mesh was used for the sampling of the Brillouin zone.

3. Results and Discussion

3.1 Synergetic Codoping Effects of Group IV-VI Impurity Pairs on BP

Impurities can break the symmetry of the hexagonal BP and inject excess carriers. The band structure can be modulated. Group IV impurity doping will result in *p*-type blue phosphorene whereas Group IV impurity doping results in *n*-type blue phosphorene. Recently, the substitutional doping of graphene with Ge was realized through ion implantation.[11]

If the blue phosphorene is codoped by both donors and acceptors, the carriers will annihilate each other. The Ge-Se and Sn-S impurity pairs doping effects on blue phosphorene was investigated. Ten configurations were considered as shown in Figure 1a. The group IV atom is fixed in “0” site and group VI atom can occupy the “1~11” sites. These 11 configurations correspond to 11 different impurity distances. The configuration dependent total energies are shown in Figure 1b. As the distance between group IV and VI atoms increases, the total energy increases. The group IV and VI atoms are charged due to the electronegativity difference between impurities and P atoms. The electronic interactions between the impurities follow the Coulomb’s law as shown by the good fit of *1/r* potential energy in Figure 1b. The S and Se atoms attain respectively 0.41 and 0.35 *e* from the

Bader charge analysis while Sn and Ge atoms lose respectively 2.18 and 2.09 *e*. The group IV-VI nearest-neighboring impurity pair is the most stable configuration, named configuration 1. For single layer 2D materials, the electric screen effects are weak, and the potential from the substituted impurities is the Coulomb electrostatic type. The calculated band structure for Ge-Se impurity pair doped BP is shown in Figure 1c that becomes a direct band gap semiconductor. Similar result was found for Sn-S doped BP (See Figure S1 of Supporting Information). The IV-VI dopant pairs create shallow impurity bands which strongly modify the electronic structures near the Fermi level. Both the valence band maximum (VBM) and conduction band minimum (CBM) move to Γ point. Meanwhile the band gaps of Ge-Se and Sn-S impurity pairs doped blue phosphorene are reduced to 1.58 and 1.51 eV respectively. Compared to the pristine blue phosphorene's value (1.89 eV), the band gaps are reduced by 0.31 and 0.38 eV respectively. The electronic affinity and work function (Φ) has also been modified by the IV-VI impurity pairs doping. The Φ of pristine BP monolayer is 5.73 eV and it is reduced by 0.27 and 0.34 eV for the Ge-Se and Sn-S impurity pairs respectively. The Φ is defined by

$$\Phi = E_{vac} - E_F \qquad (1)$$

where E_{vac} and E_F are respectively the vacuum energy and the Fermi level.[12] For strongly compensated semiconductor, the Fermi level can be expressed as $E_F = \frac{-Ce^2 N_D^{\frac{1}{3}}}{\kappa(1-K)^{\frac{1}{3}}}$, where *C* is a constant and κ is the dielectric constant and $K = N_D / N_A$.[13]

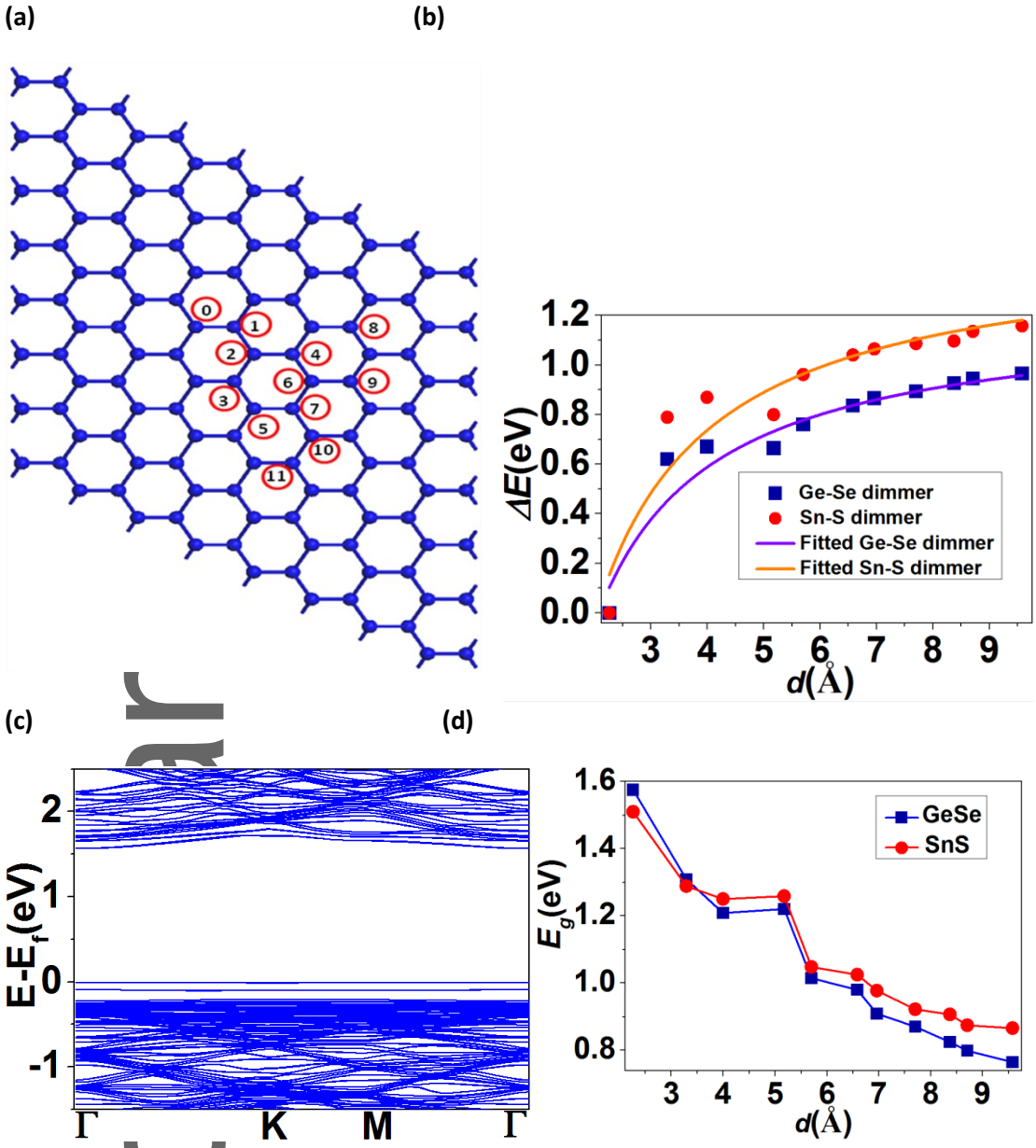

Figure 1. Structural and electronic properties of group IV-VI impurity pairs codoped BP. (a) Schematic diagram of eleven configurations of group IV-VI impurity pair codoped BP (group VI impurities are fixed at site 0 whereas group IV impurities vary from sites 1 to 11); (b) Relative total energies of doped BP versus the separation of impurity pairs (solid lines are fitted curves); band structures of (c) Sn-S and (d) Ge-Se impurity pair substitutionally codoped BP.

The group IV and VI impurity contributes shallow impurity bands at the band edges. The group IV atoms interact very strongly with the host P atoms. The strong interaction widens the valence band by pushing the VBM to the forbidden gap that, in turn, reduces the band gap. To analyze the orbital

composition of the bands close to the gap, we project the electronic states onto the atomic orbital wave functions. The decomposition of Bloch wave functions to atoms yields $|\Psi^{VBM}(\Gamma)>= 0.51|Ge->+0.86|P>$ at the Γ point. The P_z orbitals contribute the largest but not the sole contribution to VBM, which reflects the mixed sp^2 and sp^3 hybridization feature of BP. The relevant bands represent a mixture of all the orbitals, with the exception of $|p_{Ge,y}>$ having zero contribution at Γ. Since the VBM has the strong orbital contribution from Ge orbitals, it was raised up obviously and yielded the reduction of work functions. To understand the strong transfer of the CBM, the decomposition to atms yields $|\Psi^{CBM}(\Gamma)>= 0.38\ |Se>+0.92|P>$ at the Γ point. Although the p_z orbital has the largest contribution in both cases, the role of the other orbitals in the formation of CBM can't be considered as negligible. Based on the analysis of work function and band gap, the VBM and CBM are pushed up 0.27 and down 0.04 eV respectively for GeSe impurity pair doped BP. Similarly, the VBM and CBM are pushed up 0.34 and down 0.04 eV respectively for SnS impurity pair doped BP. Thus Sn atom has the stronger effects in pushing up the VBM due to its stronger metallicity compared to Ge.

The configuration-dependent band gaps are shown in Figure 1d. The general trend is that the larger the distance between the group IV and VI impurities is the smaller the band gap will be. The band gap fit well with $E_g=\sigma/r+E_0$. The σ and E_0 are 2.39 eVÅ and 0.58 eV respectively for Ge-Se doped BP and the relative standard relative deviations (RSDs) are 9.39 and 8.41 percents respectively. For Sn-S doped BP, the σ and E_0 are1.95 eVÅ and 0.71eV with the RSDs of 10.03 and 6.71 percents respectively. Both the formation energy and band gap are in the approximate Coulomb's law on the separation of group IV and VI impurities. The interactions between the charged impurities can be described by $Ze^2/4\pi\kappa r^2$. For both the formation energy and band gap curves, configuration 5 distinctly deviates the Coulomb's law. The band gap engineering through Coulomb interaction is realized in MoS_2.[14] Both the band gaps of Armchair and zigzag phosphorene nanoribbons can be reduced by the GeSe doping (See Figure S2 of Supporting Information).

3.2. Concentration-Dependent Doping Effects of Group IV-VI Impurity Pairs on BP

To further enhance the modification of the electronic structures, we increase the impurity concentration. M_nX_n (M=Ge, Sn; X= S, Se) clusters are used to dope the BP. The formation energies are calculated to study the stabilities of the modified BP. The formation energy is defined as follows

$$\Delta H_f(M) = E_{tot}(M) - E_{tot}(clean) - \sum_i n_i\mu_i \qquad (2)$$

where $E_{tot}(M)$ is the total energy of the chemically modified BP and $E_{tot}(clean)$ is the total energy of the clean BP. μ_i denotes the chemical potential for species *i* (host atoms or dopants) of the crystalline bulks, and n_i the corresponding number that have been added to or removed from the supercell. As the size of the M_nX_n clusters increases, the formation energy decreases as shown in Figure 2a. Based on the analysis of the differential of $d[\Delta H_f(M)]/dn$, the values of M_5X_5, M_8X_8, $M_{12}X_{12}$ and $M_{27}X_{27}$ are the local minimums, due to the closed-shell hexagonal edges. Interestingly, similar magic hexagonal cluster C_{24} plays important role in graphene growth on metal substrate.[14] From the view point of the 2D crystal nucleation and growth, the formation energies of MX clusters can be attributed to two factors: the edge formation energy and chemical potential variation due to the new phase formations. Accordingly, the formation energies can be expressed as:

$$\Delta H_f = l\gamma + n\varepsilon \quad (3)$$

Where *l* is the length of the edge of M_nX_n clusters; *n* is the number of M-X impurity pairs. In fact, the embedded clusters may endure the residual strain which will increase the formation energy. Neverthless, this simplified model can be used to understand the initial nucleating and growth of the embedded clusters. Fit our results by Eq. (3), we have γ=0.67 eV/nm and ε=-0.41 eV for embedded Ge_nSe_n clusters and γ=0.76 eV/nm and ε=-0.77 eV for embedded Sn_nS_n clusters. Thus the larger edge length of the embedded clusters will result in larger formation energy and the lower stability.

As shown in Figure 2b, the nonlinear impurity pair concentration dependence of band gap is found and the general trend is that the larger the impurity concentration is the smaller the band gap will be. The doped BP can be denoted as $P_{1-\chi}M_{\chi/2}X_{\chi/2}$. The band gap reduction effects of BP on the doping by IV-VI clusters can be described by the modified Vegard's model based on virtual crystal approximation[7,16] as following equation.

$$E_g = E_{BP}(1-\chi) + E_{MX}\chi - b\chi(1-\chi) \quad (4)$$

Where χ is the concentration of the impurity; E_{BP} and E_{MX} are the band gaps of BP and 2D MX respectively; *b* is the band gap bowing parameter. The band gaps are 2.69 and 2.37 eV for 2D hexagonal SnS and GeSe respectively. The fitted bowing parameter *b* is around 3.69 and 4.68 eV for GeSe and SnS respecively. Strictly speaking the bowing parameter is concentration-dependent and it can be solved by Eq. (4). These large bowing parameters can be attributed to the structural relaxation effects and strong orbital hybridization between IV-VI impurity pairs and BP. IV-VI clusters

are of the impurities for the shallow levels that contribute importantly to the DOS at both VBM and CBM.

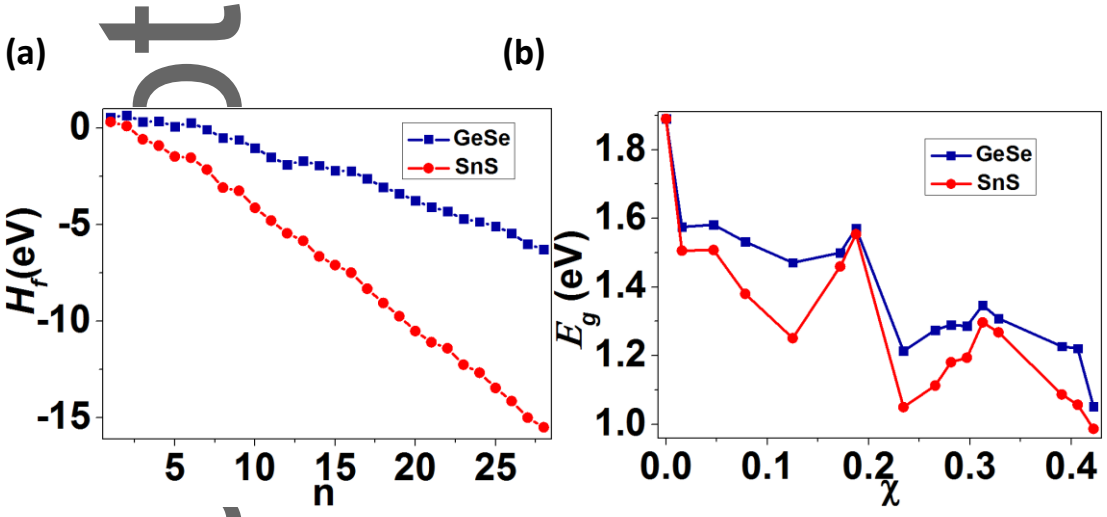

Figure 2. Formation energies and band gaps of M_nX_n clusters doped BP. (a) Formation energies versus the sizes of the doped M_nX_n clusters. (b) Band gap versus the impurity concentration χ, which is defined as χ = n/64.

Other MX doped BP effects are investigated. The optimized structures of hexagonal $M_{12}X_{12}$ and $M_{27}X_{27}$ clusters modified BP by GeSe and SiS are shown in Figs. 3a~3d. SiS, have a tiny lattice mismatch (0.6 percent) with BP since Si and S are the nearest-neighboring elements of P. Thus there is weak strain in BP induced by SiS doping. The structural distortion induced by SiS is weaker than that induced by GeSe. The inversion and three-fold rotational symmetries of BP are broken. With the MX doping, the band gap of BP is remarkably reduced. The band gaps for $Si_{12}S_{12}$ and $Ge_{12}Se_{12}$ modified BP are respectively 1.56 and 1.57 eV as shown in Figs. 3e and 3f. As the doping concentration is increased, the band gaps are further reduced to 1.20 and 1.05 eV respectively for $Si_{27}S_{27}$ and $Ge_{27}Se_{27}$ modified BP as shown in Figs. 3g and 3h respectively.

To study different IV-VI impurity pair doping effects, a series of MX clusters are explored. Two typical doping configurations are considered: hexagonal M_3X_3 doped BP 5×5 cells and hexagonal $M_{27}X_{27}$ doped BP 8×8 cells. The corresponding impurity concentrations are 12 and 42 percents respectively. The impurity pair doping dependent band gaps are shown in Figure 3i. GeS and PbTe have respectively weakest and strongest doping effects on the band gap of BP. Though GeS is an exception, the general doping trend is that the heavier the impurity pair is the stronger the tuning

effects will be. This can be attributed to that the metallicity of the atoms in the same group is enhanced as the number of rows is increased. The metallicity of Si, Sn and Pb is stronger than P. The electronegativity of S is stronger than P, wheras the electronegativity of Te is weaker than P. Se is the nearest-neighboring diagonal element of P. Through the stronger metallic impurities doping, the delocalization of BP is increased. Hence the band gap can be reduced. The doping via PbTe clusers even induces the semiconductor to metal transition of BP.

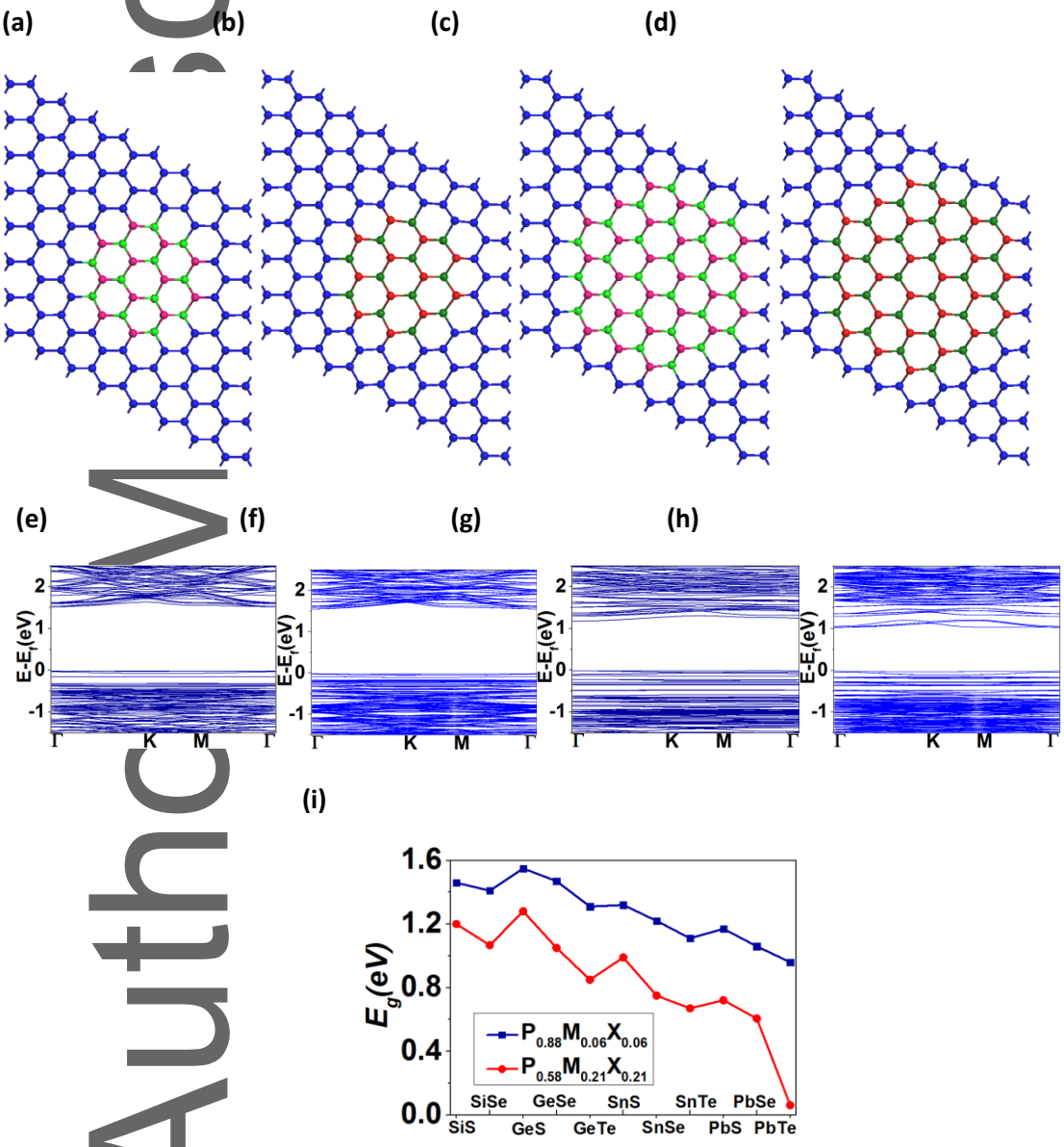

Figure 3. Optimized structures and electronic properties of hexagonal M_nX_n clusters doped BP. Structures of (a) $Si_{12}S_{12}$, (b) $Ge_{12}Se_{12}$, (c) $Si_{27}S_{27}$ and (d) $Ge_{27}Se_{27}$ doped BP. Band structures of (e) $i_{12}S_{12}$, (f) $Ge_{12}Se_{12}$,

(g) $Si_{27}S_{27}$ and (h) $Ge_{27}Se_{27}$ doped BP. (i) Impurity dependent band gaps at two fixed impurity concentrations.

3.3 Configuration-Dependent Electronic Properties of Doped BP

To clarify the correlations between structures and the electronic properties, a series of configurations of $Ge_{12}Se_{12}$ clusters doped 8×8 BP are considered. The structures can be expressed as $P_{1-\chi}Ge_{\chi/2}Se_{\chi/2}$ with the χ of 0.188. Six calculated representative configurations are shown in Figure 4. From the view point of thermodynamics, the alloyed structures are not stable compared to the clustering configuration due to higher formation energy. Phase separation is a common phenomenon in the semiconductor doping. Nevertheless their electronic structures need to be revealed to fully understand the band gap modulation mechanism. The real doped BP structures can be controlled by the kinetic methods such as above eutectic melting temperature, suitable stoicheiometry, pressure, ultrasonics, charges etc in the experiments. For Figure 4a and 4b, the impurities are in the formula of close-shelled hexamer configurations. The band gaps are 1.47 and 1.50 eV respectively. These values don't differ obviously with that of clustering configuration as shown in Figure 3b (1.57 eV). In Figure 4a, the Ge_3Se_3 hexamer is uniformly distributed and it is randomly distributed in Figure 4b. Calculated GeSe dimmer configurations are shown in Figs. 4c and 4d. The corresponding band gaps are 0.63 and 0.96 eV respectively. Thus configurations have strong influence on the electronic properties. If the impurity clusters are uniformly distributed, the band gaps can be remarkably reduced. Furthermore, the alloyed BP with $Ge_{12}Se_{12}$ impurities is studied as shown in Figure. 4e and 4f. The corresponding band gaps are 0 and 0.53 eV respectively. Thus the band gaps of BP can be easier controlled through the alloyed doping formula. Doped BP with the alloyed structures undergoes the semiconductor to metal transition. The band structures for configurations 4a, 4c and 4e are shown in Figure 4g, 4h and 4i respectively and they exhibit the direct band gap characteristics. Due to the presence of time-reversal symmetry, the Rashba-like spin-split can't be realized at Γ point. However the 7 meV spin-split is realized at K point in the vicinity of 0.2eV above Femi level as shown in Figure 4i. For the six configurations listed in Figure 4, SOC is found to reduce the band gaps in the range of 4~11 meV by comparing the band structures w/ and w/o considering SOC effects.

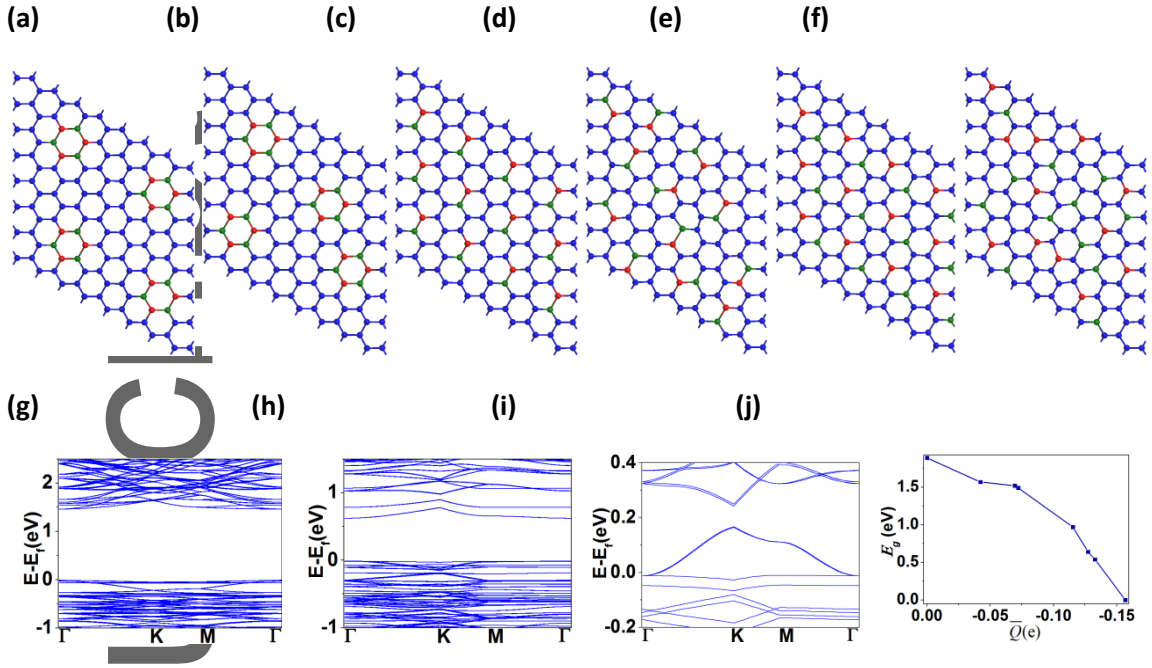

Figure 4. Optimized Structures and configuration-dependent electronic properties of $Ge_{12}Se_{12}$ doped 8×8 BP. (a) and (b) Ge_3Se_3 hexamer configurations; (c) and (d) GeSe dimmer configurations; (e) and (f) alloy configurations. (g) Band structures of configuration a. (h) Band structures of configuration c. (i) Band structures of configuration e. (i) Averaged charge dependent band gap.

For the alloyed configurations, the group IV and VI impurities are surrounded by the host P atoms and they play effectively the roles as acceptors and donors. The Se-P bond has an excess unpaired electron which is more delocalized than the paired electrons. Meanwhile Ge is a p-type impurity which induce a hole carrier. The alloyed structures can maximally benefit the conductivity and the semiconductor to metal transition is reached. The configuration-dependent band gap characteristics of $Ge_{12}Se_{12}$ doped 8×8 BP can be understood by the Anderson disorder model. The periodicity of the Bloch wavefunction of BP is locally destroyed by the impurities. The wavefunction of impurity electron is in the formula of exp(-r/ξ) where ξ is the localization length. For the alloy configurations, the impurities are more continuously distributed compared to clustering, hexamer and dimmer configurations. This is propitious to the extending of the wavefunctions of the impurities. The charge transfer between impurities and BP is analyzed. The charge transfer can induce variation of the on-site energy and additional coulomb potential to the Hamiltonian. The charge transfer (*Q*) between BP and $Ge_{12}Se_{12}$ impurities is in the range of 5.4~20.1 *e* and BP gains the charges from the impurities. The charge transfer of configurations in Figures 3b, 4a and 4e is 5.4, 8.9 and 20.1 *e*. The Band gap versus the averaged charge $\overline{Q}$ (*Q*/P atom) is shown in Figure 4j. The band gap is reduced as the $\overline{Q}$ is

increased. The value of $\overline{Q}$ reflects the degrees of the hybridization effects between the impurities and BP. In addition, $\overline{Q}$ will also induce the Coulomb interactions and change the on-site energies of the Hamiltonian. Different configurations of doped structures result in the band gap difference as large as 1.57 eV which reflects the importance of the structures. The band gap bowing parameters is not only concentration-dependent but also configuration-dependent. The bowing parameters is in the range of 4.30~22.73 eV for configurations 4a~4f. The huge bowing parameter indicates the strong tuning effects through the doping of GeSe. The similar effects are found for SnS doped BP.

3.4. Synergetic Codoping Effects on BP Quantum Dots

Since the BP quantum dots (QDs) with sizes of several nm have been fabricated in the experiments, [2,17] it is important to investigate the interactions between group IV-VI impurities and BP quantum dots. The hexagonal BP cluster with the size of 3.2 nm is considered, which contains 150 P atoms as shown in Figure 5a. The edges of BP clusters are saturated by H atoms to eliminate the dangling bonds. A series of compensated IV-VI clusters are considered with the concentration of 1.33~98.67 percents. The structures of GeSe, Ge_3Se_3, $Ge_{12}Se_{12}$ and $Ge_{27}Se_{27}$ doped BP QD is shown in Figs. 5b~5e. The pristine BP quantum dot has the energy gap of 2.25 eV which is 0.36 eV larger than that of monolayer BP due to the quantum confinement effects and Coulomb interaction as shown in Figure 5f. The electrons are confined in all three directions and more localized compared to these of monolayer. The energy gap of quantum dot can be described by $E_{QD}= E_0+a/r+b/r^2$, where the first, second and third terms represent the monolayer band gap, Coulomb interaction energy and kinetic energy determined by quantum confinement effect. Quantum confinement effect enlarges the gap and the Coulomb interaction is strengthened with decreasing size of QDs. By GeSe impurity pair doping, the band gap is reduced to 1.71 eV as shown in Figure 5g. This impurity pair breaks the inversion and three-fold rotational symmetries. This impurity pair induces the band gap reduction of 0.54 eV. The Ge impurity modifies the HOMO orbital and the wavefunction at HOMO can be decomposed as $|\Psi^{HOMO}>= 0.48|Ge>+0.88|P>$. Meanwhile, the decomposition at LUMO yields $|\Psi^{LUMO}>= 0.45|Se>+0.89|P>$. Ge and Se impurities modify the HOMO and LUMO respectively. The work function of pristine $P_{150}H_{30}$ QD is 5.21 eV and it has been reduced by 0.24 eV through Ge_1Se_1 doping which is comparable to the Φ reduction of BP monolayer by Ge_1Se_1 (0.27 eV). The Ge impurity raised up the HOMO by 0.24 eV meanwhile the Se impurity lowered down the LUMO by 0.30 eV. For the Ge_3Se_3 doped BP QD, Ge and Se impurities contribute the DOS to HOMO and LUMO respectively. The energy gap is reduced to 1.78 eV as shown in Figure 5h. Actually, the energy gap is

configuration-dependent and the values is in the range of 0.08~1.78 eV (see Figure S3 of Supplemental Material).

The concentration-dependent band gap is shown in Figure 5i. For Ge_1Se_1 and Sn_1S_1 doped BP, the band gaps are in the range of 1.36~2.25 and1.10~2.25 eV respectively. The minimum band gaps can be reached with the impurity concentration of 0.84. The energy gaps of hexagonal $Ge_{75}Se_{75}$ and $Sn_{75}S_{75}$ QDs are 1.45 and 1.27 eV respectively. The band gap bowing can be described by the Eq. (4). For the χ of 1.33 and 4.0 percents, the giant band gap bowing parameters are obtained with the values of 40.2 and 11.7 eV respectively according to the Eq. (4). The band gap differences ΔE_g of w/ and w/o SOC are in the range of 0~11 and 0~15 meV for GeSe and SnS doped BP QDs respectively. The corresponding impurity concentrations for the largest ΔE_g are 84 and 36 percents for GeSe and SnS doping respectively. The SOC contribution to the Hamiltonian can be described as $H_{SO}= \lambda_{SO}\boldsymbol{L}\cdot\boldsymbol{S}$, where λ_{SO}, ***L*** and ***S*** are the strength of the SOC, orbital and spin angular momentums respectively. The SOC can induce the perturbations which will break the spin degeneracy and narrow down the energy gaps of quantum dots. [18] Te and Pb impurities can induce stronger SOC in BP.

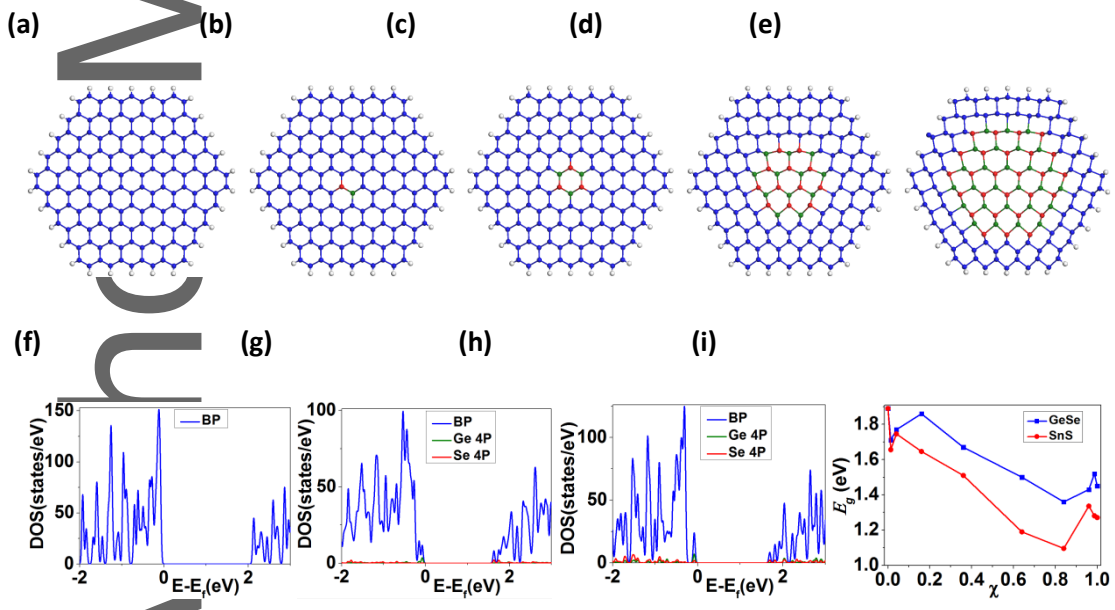

Figure 5. Structural and electronic properties of pristine and Ge_nSe_n doped BP. Structures of (a) pristine, (b) GeSe, (c) Ge_3Se_3, (d) $Ge_{12}Se_{12}$ and (e) $Ge_{27}Se_{27}$ doped BP QDs. DOS of (f) pristine, (g) GeSe, (h) Ge_3Se_3 doped BP QDs. (i) Impurity concentration-dependent band gap.

4. Conclusions

In summary, the electronic structures of BP can be effectively modulated by the synergetic codoping of group IV and VI impurities. The indirect to direct band gap transition is realized. Strong band gap bowing is found in all monolayer, nanoribbons and QDs. Coulomb interactions between impurities are revealed. SOC can also be tuned by the incorporation of the impurities. This effective modulation avenue of electronic structures can be applicable to other two-dimensional materials.

Supporting Information

Supporting Information is available from the Wiley Online Library or from the author.

Acknowledgements

This work was supported the NSFC (11774296, 11574217, 11734012, 11574218 and 11504241), NSF of Guangdong (2018A0303130311 and 2016A030313059), Science and Technology plan project of Guangdong (2017A010101018), Science and Technology plan project of Shenzhen (JCYJ201811915, JCYJ20180305300026 6, JCYJ20160307142444674 and JCYJ20160307111047701), the Hong Kong RGC (16300117 and 16301816). B.I.Y. was supported by the Army Research Office (W911NF-16-1-0255), the Office of Naval Research (N00014-15-1-2372), US Department of Energy (DE-SC0012547) and by the R. Welch Foundation (C-1590).

Keywords:

Blue phosphorene· synergetic codoping· density functional calculations· band gap bowing· Coulomb interactions

[1] Z. Zhu, D. Tománek, *Phys. Rev. Lett.* **2014**, 112, 176802.

[2]a) J. L. Zhang, S. T. Zhao, C. Han, Z. Z. Wang, S. Zhong, S. Sun, R. Guo, X. Zhou, C. D. Gu, K. D. Yuan, Z. Y. Li, W. Chen, *Nano Lett.* **2016**, 16, 4903-4908.b) C. D. Gu, S. T. Zhao, J. L. Zhang, S. Sun, K. Yuan, Z. H. Hu, C. Han, Z. R. Ma, L. Wang, F. W. Huo, W. Huang, Z. Y. Li, W. Chen, *ACS Nano* **2017**,11, 4943-4949 c) J. C. Zhuang, C. Liu, Q. Gao, Y. N. Liu, H. F. Feng, X. Xu, J. O. Wang, J. J. Zhao, S. X. Dou, Z. P. Hu, Y. Du, *ACS Nano* **2018**,12, 5059-5065.

[3] L. Tao, E. Cinquanta, D. Chiappe, C. Grazianetti, M. Fanciulli, M. Dubey, A. Molle, D. Akinwande, *Nat. Nanotechnol.* **2015,**10 ,227-231.

[4]a) Z. C. Zhang, L. K. Li, J. Horng, N. Z. Wang, F. Y. Yang, Y. J. Yu, Y. Zhang, G. R. Chen, K. Watanabe, T. Taniguchi, X. H. Chen, F. Wang, Y. B. Zhang, *Nano Lett.* **2017**, 17, 6097-6103.b) A. S. Rodin, A. Carvalho, A. H. Castro Neto, *Phys. Rev. Lett.* **2014**,112, 176801.c) R. X. Fei, L. Yang, *Nano Lett.* **2014,**14, 2884-2889.

[5]a) S. P. Koenig, R. A. Doganov, L. Seixas, A. Carvalho, J. Y. Tan, K. Watanabe, T. Taniguchi, N. Yakovlev, A. H. C. Neto, B. Özyilmaz, *Nano Lett.* **2016,**16, 2145-2151.b) J. Kim, S. S. Baik, S. H. Ryu, Y. Sohn, S. Park, B. G. Park, J. Denlinger, Y. Yi, H. J. Choi, K. S. Kim, *Science* **2015**,349, 723-726.c) Y. C. Cheng, Y. H. Zhu, Y. Han, Z. Y. Liu, B. C. Yang, A. Nie, W. Huang, R. S. Yassar, F. Mashayek, *Chem. Mater.* **2017**,29, 1350-1356.d) S. Y. Cho, H. J. Koh, H. W. Yoo, H. T. Jung, *Chem. Mater.* **2017**,29, 7197-7205.

[6] B. Huang, M. Yoon, B. G. Sumpter, S. H. Wei, F. Liu, *Phys. Rev. Lett.* **2015**,115, 126806.

[7]a) C. Persson, C. Platzer-Björkman, J. Malmström, T. Törndahl, M. Edoff, *Phys. Rev. Lett.* **2006**,97, 146403. b) A. Rubio, M. L. Cohen, *Phys. Rev. B* **1995**,51, 4343-4346.c) S. H. Wei, A. Zunger, *Phys. Rev. Lett.* **1996**,76, 664-667.d) V. R. D'Costa, Y. Y. Fang, J. Tolle, J. Kouvetakis, J. Mene´ndez, *Phys. Rev. Lett.* **2009**, 102, 107403.e) B. Fluegel, S. Francoeur, A. Mascarenhas, S. Tixier, E. C. Young, T. Tiedje,*Phys. Rev. Lett.* **2006**,97, 067205.

[8] a) Z. Tian, C. L. Guo, M. X. Zhao, R. R. Li, J. M. Xue, *Acs Nano.* **2017**,11, 2219-2226. b) D. J. Xue, S. C. Liu, C. M. Dai, S. Y. Chen, C. He, L. Zhao, J. S. Hu, L. J. Wan, *J. Am. Chem. Soc,* **2017**,139, 958-965.c) A. J. Biacchi, D. D. Vaughn, R. E. Schaak, *J. Am. Chem. Soc.* **2013**,135,11634-11644.d) L. Li,

Z. Chen, Y. Hu, X. W. Wang, T. Zhang, W. Chen, Q. B. Wang, *J. Am.Chem. Soc.* **2013**,135, 1213-1216.

[9] P. Giannozzi, S. Baroni, N. Bonini, M. Calandra, R. Car, C. Cavazzoni, D. Ceresoli, G. L. Chiarotti, M. Cococcioni, I. Dabo, A. D. Corso, S.D. Gironcoli, S. Fabris, G. Fratesi, R. Gebauer, U. Gerstmann, C. Gougoussis, A. Kokalj, M. Lazzeri, L. Martin-Samos, N. Marzari, F. Mauri, R. Mazzarello, S. Paolini, A. Pasquarello, L. Paulatto, C. Sbraccia, S. Scandolo, G. Sclauzero, A. P. Seitsonen, A. Smogunov, P. Umari, R. M. Wentzcovitch, *J. Phys.: Condens Matter* **2009,**21, 395502.

[10] J. P. Perdew, K. Burke, M. Ernzerhof, *Phys. Rev. Lett* **1996**,77, 3865-3868.

[11] M. Tripathi, A. Markevich, R. Böttger, S. Facsko, E. Besley, J. Kotakoski, T. Susi, *ACS Nano.* **2018,**12, 4641-4647.

[12] Y. M. Li, J. Li, L. K. Shi, D. Zhang, W. Yang, K. Chang, *Phys. Rev. Lett* **2015**, 115,166804.

[13] B. I. Shklovskiĭ, A. L. Éfros, *Sov. Phys. JETP.* **1972**,35, 610-614.

[14] A. Raja, A. Chaves, J. Yu, G. Arefe, H. M. Hill, A. F. Rigosi, T. C. Berkelbach, P. Nagler, C. Schu¨ller, T. Korn, C. Nuckolls, J. Hone, L. E. Brus, T. F. Heinz, D. R. Reichman A. Chernikov, *Nat. Commun* **2017,**8, 15251.

[15] Q. H. Yuan, J. F. Gao, H. B. Shu, J. J. Zhao, X. S. Chen, F. Ding, *J. Am. Chem. Soc.* **2012,**134, 2970-2975.

[16] S. Adachi, *Properties of Semiconductor Alloys: Group-IV, III-V and II-VI Semiconductors.* Wiley, Chichester, **2009**.

[17] J.-P. Xu, J.-Q. Zhang, H. Tian, H. Xu, W. K. Ho, M. H. Xie, *Phys. Rev. Mater.* **2017**, 1, 061002.

[18] A. Kormányos, V. Zólyomi, N. D. Drummond, G. Burkard, P*hys. Rev. X.* **2014**,4, 011034.

Table of Contents (TOC)

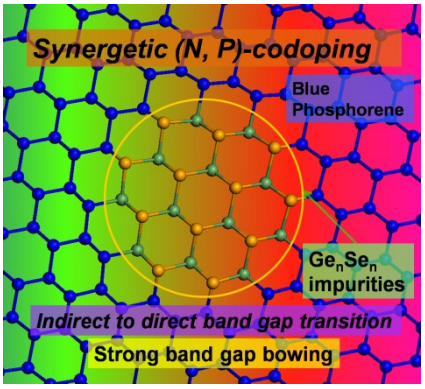

The band structure of blue phosphorene (BP) is engineered through synergetic codoping with group IV and VI impurities. The indirect to direct band gap transition is found. The band gap of BP can be modulated in a wide range, and strong band gap bowing is found. Lower formation energies indicate the fabricating practicability.